https://doi.org/10.20965/jrm.2013.p0097

Paper:

Development of Microscopic Hardness and Stiffness Investigation System with Microrobot 2nd Report, Vision Based Precise Navigation

Montree Pakkratoke*, **Shinnosuke Hirata****, **Chisato Kanamori***, **and Hisayuki Aoyama***

*Department of Mechanical Engineering and intelligent systems, The University of Electro-Communications
1-5-1 Chofugaoka, Chofu, Tokyo 182-8585, Japan
E-mail: montree@nimt.or.th, {kanamori, aoyama}@mce.uec.ac.jp
**Department of Mechanical and Control Engineering, Tokyo Institute of Technology
2-12-1 Ookayama, Meguro, Tokyo 152-8552, Japan
E-mail: shin@ctrl.titech.ac.jp

[Received April 6, 2012; accepted May 17, 2012]

A microsurface measurement system that is composed of the microrobot with the indenter and a vision based navigation system is proposed for investigating hardness and stiffness of such microparts. Here the tiny robot with the electromagnetic legs and the piezo elements incorporates with an electromagnetic driven microforce generator. This force generator can provide small forces up to 17 mN with 50 μN resolutions and push down the microindenter to the surface. The displacement of the indenter head can be also measured by the Linear Valuable Differential Transformer (LVDT) on machine. Thus, this mechanism can generate the small force and monitor the depth behaviour of the indenter during whole dwell time. Since the overall size of this mechanism is small enough to implement on the piezo-driven microrobot, the tiny robot with the microindenter is capable to move precisely step by step with 1 μm per step so that the microindenter could be penetrated anywhere on the sample surface. With the help of an image processing technique, the vision based coordination system with the local close-up view and the overall global view has been developed to identify the locations of small robot and the indenter precisely within ± 3 μm accuracy over the working range. In the experimental results, several results that the indentation load-depth characteristics of the unhealthy human tooth are measured automatically at the specified point are discussed.

Keywords: microforce actuator, piezo-driven inchworm robot, microindenter, vision based navigation system

1. Introduction

Material selections in engineering applications are very crucial. Engineers have to confirm that material properties are appropriate for the operational condition. There are many kinds of material properties; an ultimate tensile strength is one of the most useful properties for predicting the strength of material. Regarding to tensile testing method, a testing material must be destroyed; which it is not appropriate in some situation. In additional there is another way to predict a strength property of materials without large damage to a test sample, that is a hardness test. The previous works [1–3] have shown relation between the hardness value and the ultimate tensile strength. The hardness test has been widely used for nearly 100 years, because the indentations are very small and the surface quality of material is not destroyed. This technique is considered to be non-destructive test method. Recently, the size of materials and machined components to be checked keep decreasing because high density with down-sizing trends. In term of traditional hardness testing methods, the indentation depth or the dimension size of the indenter imprint is used for calculate the hardness value. The accuracy of hardness value depends upon a measuring device. For such microscale materials or bio materials, the application force of hardness testing should be very low because the stiffness of these materials are also very low. Therefore, the traditional hardness testing machine is difficult to obtain good accuracy of material properties. For this reason, an instrumented indentation testing is becoming very important for determining the mechanical properties of such bio materials especially materials in microscales. An instrumented indentation testing method is similar to a traditional hardness test in that pressing an indenter of known geometry and mechanical properties under pre-defined conditions into the test material. It can provide a continuous record of a variation of a testing force as a function of the indentation depth when the indenter is penetrated into the specimen. The slope of unload curve has commonly been used to calculate an elastic modulus [4, 5]. In order to achieve such microhardness test, the loading force of an indenter should be precisely applied to the material without any shock or vibration. There are a number of mechanisms and methods for a nano and micro range force generator such as applying force using a coil of wire inserted into a

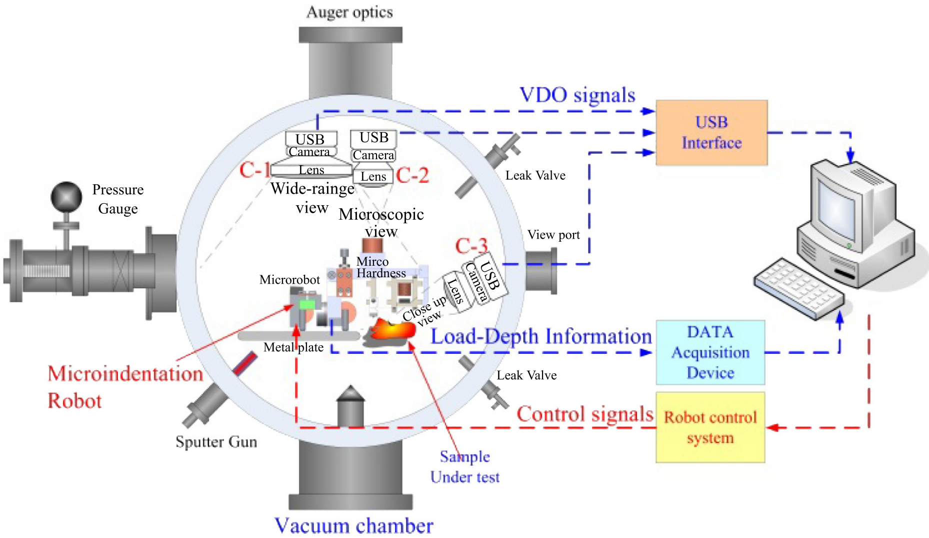

Fig. 1. Microdiagnostics robot with hardness and stiffness testing navigation based on multiple vision images.

cylindrical slot in a permanent magnet [6], electrostatic force [7], a spring method [8]. On previous work [9], we succeed in the development of the first prototype of a microindentation robot. This is the combination of the tiny piezo-driven microrobot and the small hardness testing mechanism. Here the small mechanical loop can provide the benefits of low thermal expansion and higher mechanical stiffness as well as the self-walking robot can expand the working range. It can investigate the microscopic elastic behaviors of certified hardness blocks by determining the indentation load-depth curves. Although it can be operated without a position control system, the indentation pattern cannot be precisely controlled along the specified path. In this paper the conceptual view of the down-sized instrumentation microhardness and stiffness measuring robot with the position control by multi vision images navigation is presented as shown in **Fig. 1**.

This paper is organized as follows. Sections 2 introduce the vision based navigation system for tracking and controlling a microrobot position with high precise movement. Section 3 describes the robot position control using the vision based navigation system, including the path control under wide range and microscopic views respectively. Section 4 presents the performance of the robot tracking system, including the repeatability experimental results of this navigation system. Furthermore, the performance of the instrumented indentation testing robot with the experiments on a human tooth inside a specified measurement area is presented. The tooth surface stiffness characteristic can be identified automatically by a series of indentation load-depth along the designed robot path. Finally, Section 5 summarizes this paper and the future works.

2. Vision Based Navigation System

In the previous paper [9], a small robot with a microindenter was developed as shown in **Fig. 2**. This section is focusing on the vision based navigation system for this small robot. A primary goal of this paper is an implementation of the micro stiffness and hardness testing robot to operate inside a small chamber. Thus, small several CCD cameras with lens can be employed for real-time path control. Such a vision based sensory system [10] has been proposed for an automatic assembly operation by microrobot. In our setup, the layout of several CCD cameras is shown in **Fig. 3**. The objectives are to provide many viewpoints of a robot, a design of trajectory path and the measurement point path.

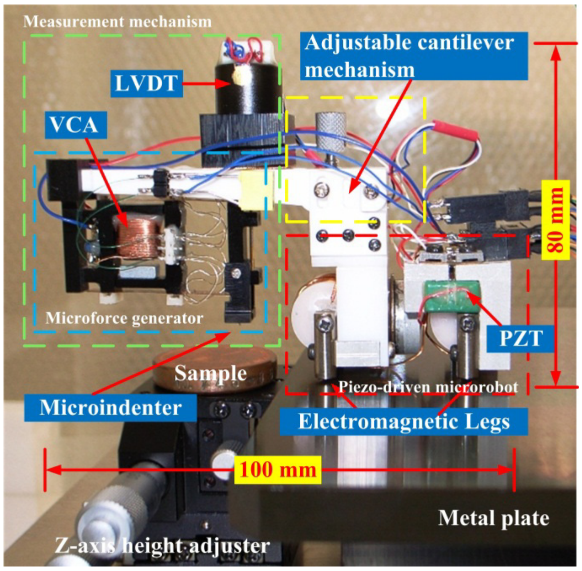

Fig. 2. The prototype of the microindentation robot.

An image processing technique used in this tracking system is the IMAQ Vision commercially supplied from National Instruments corporations (NI). The automatic color pattern matching technique is used in this system, thus a movement of a small robot can be tracked and controlled with the help of LabView. The color pattern matching is able to accurately locate the object that the size of which is varying and rotating within 360° [11]. The color pattern matching is composed of two important

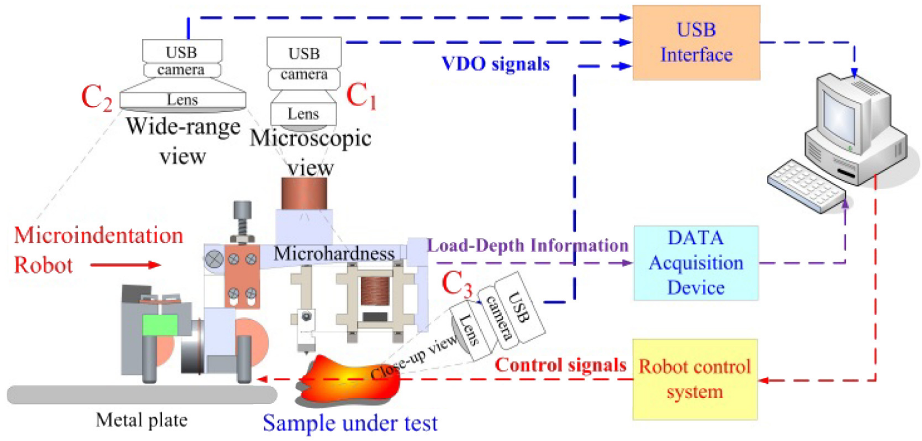

Fig. 3. Multi-cameras based coordinate system for robot navigation.

parameters, i.e., a marker and a template. With the template pattern of the marker, the template can be scanned in the image to get the matching position for shape and color sensitivity. The matching score can be determined by a comparison of color and pattern between a marker and its template. Such a score of the match is related to how accurate the pattern model matches the marker founded. The matched pattern can be marked, and the position of a marker can be identified by a coordinate pixel from the whole picture. Such coordination can be utilized as a representative of the marker position.

2.1. Experimental Setup for Calibration

Here two camera types, a high magnification type (C_1, C_3) and a wide view angle type (C_2) are employed in this tracking system as shown in **Fig. 3**. C_1 and C_2 cameras are placed on the top of the robot. C_1 camera has two operational functions. The first function is that the operator can observe a sample surface and check the interesting area. A second function is that the measured position is feed back to the controller to maneuver the robot path during a measurement process. At first, the C_1 camera can focus at a red marker placed on the center axis of LVDT case so that the indenter position can be detected. The second camera C_2 is placed next to C_1 so that it can monitor the overall behavior of the robot in the working range. Finally, C_3 camera with long working distance microscope lens is placed on the right side of robot in order to observe the behavior of the indenter tip.

Because many cameras work together but in different scale and function, before implementation of a camera system, a verification of a CCD camera pixel change due to the displacement change is required.

The experiment setup is shown in **Fig. 4**, two precision controlled X-Y stages are used as a displacement standard. A large stage has a moving range about 50 mm, while a small stage has 25 mm. both of them have same movement resolution at 1 μm per step. There are two markers placed on both stages, its shape and size are different for each camera. The cameras are setup to focus on the makers on the stage. When the stage is moving, the images of a marker monitored by a camera also move. By com-

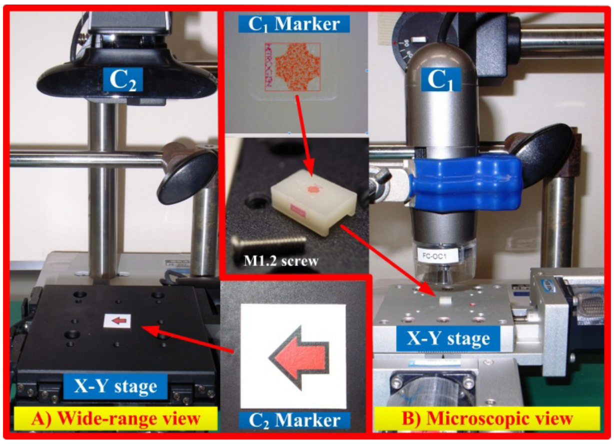

Fig. 4. Experiment setup for calibration of cameras pixel change compared with the actual movement of X-Y controlled stage, wide-range view (A) and microscopic view (B).

paring an image pixel change read out by a camera with a position of the marker on moving stage, the CCD pixel can be calibrated.

2.2. Calibration in Wide-Range View

The wide-range view (C_2 camera) is focused on a larger red arrow marker size about 10×10 mm placed on a large stage. The focusing length is fixed at 150 μm per 1 pixel. The C_2 camera has a CCD effective area at 1024×576 pixels. This implies that the operation range of C_2 is about 150×80 mm. The calibration procedure of C_2 camera is as follows, the stage is moved with 1 mm per step from 0 to 50 mm repeated ten times. Then the pixel read out from tracking software is compared with the actual stage movement. The experiment results are shown in **Fig. 5**. It is depicted that an accuracy of the tracking software with C_2 camera is achieved ± 1 pixel or about ± 150 μm.

2.3. Calibration in Microscopic View

The microscopic view (C_1 camera) focuses on a marker, the shape of which is similar to plus sign. Its

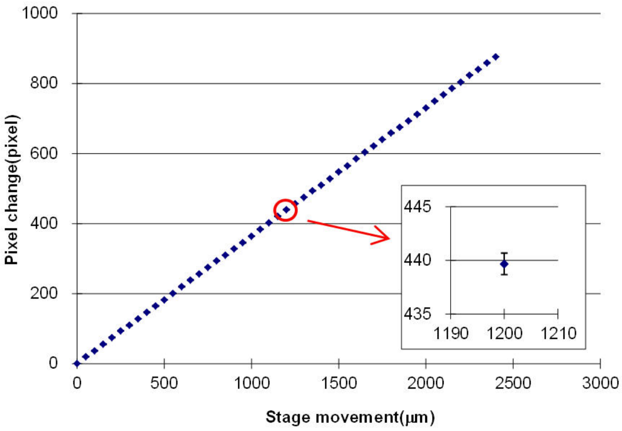

Fig. 5. Comparison results between actual movement of a marker and a pixel change of C_2 camera (wide-range view).

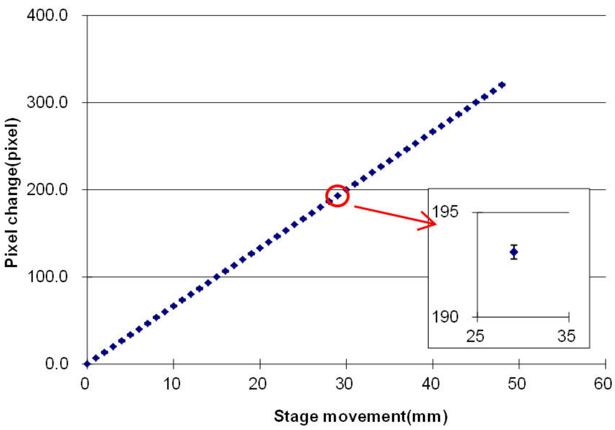

Fig. 6. Comparison results between actual movement of a marker and a pixel change of C_1 camera (microscopic view).

size is less than 1 mm, which is placed on the small X-Y stage. The focusing length is fixed at 2.5 μm per 1 pixel. The C_1 camera has 1024×576 pixels CCD effective area, which indicates that the operation range of C_1 is about 3.2×2.3 mm. The calibration procedure of C_1 camera is as follows, the stage is moved with 10 μm per step from 0 to 2.5 mm repeated ten times. Then the pixel read out from tracking software is compared with the actual stage movement as shown in **Fig. 6**. It is indicated that an accuracy of the proposed technique with C_1 camera is also achieved ± 1 pixel or about ± 2.5 μm.

The comparison results between a tracking camera and a controlled X-Y stage have shown that the accuracy is achieved ± 1 pixel on both cameras. These results have reached the limit of a CCD camera at one pixel. After that the image tracking system is implemented into the whole measurement system as shown in **Fig. 7**. The plastic chamber size is 50 cm in width, 30 cm in height and 30 cm in depth. An overall system, including the microindentation robot and the vision based tracking system is encompassed into the chamber. The working range of the camera system has been changed to make it appropriate to the chamber size, i.e., C_1 is set to 1.75 um/pixel with full operation range at 2.5×2 mm, and C_2 is set to

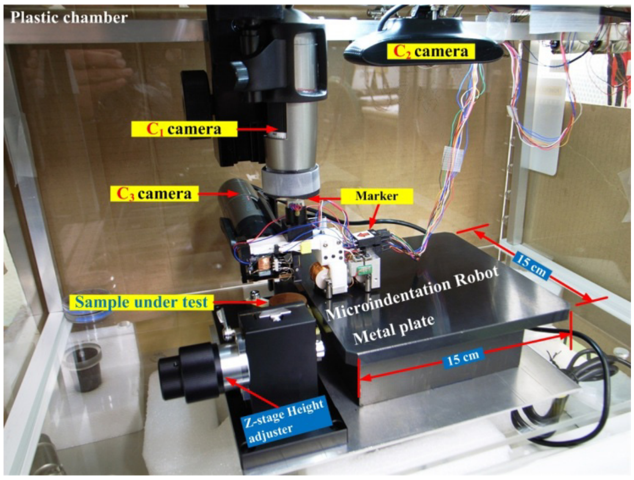

Fig. 7. The vision based navigation system of the microindentation robot with three CCD cameras in the chamber.

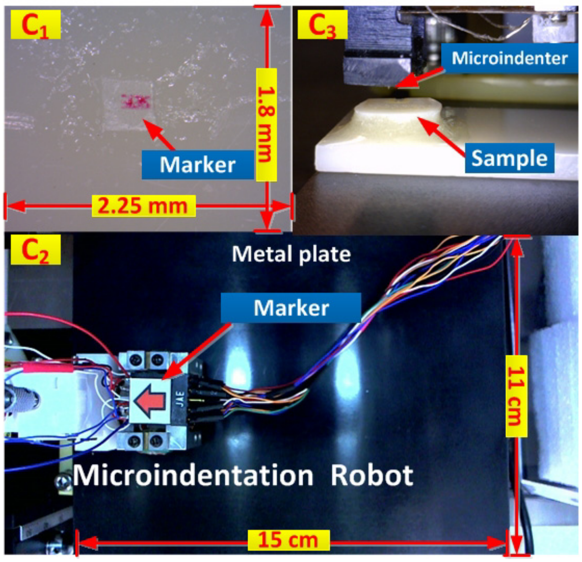

Fig. 8. Camera views and the actual scale from C_1, C_2 and C_3 in the chamber.

190 um/pixel with full operation range at 150×100 mm (**Fig. 8**). These scales come from calibration results between image pixel and standard scale after all cameras are placed in the position inside the chamber.

At this moment, the vision based position tracking system is ready to track and control a robot's position. In the next section, a surface stiffness measurement process and a robot path control will be described.

3. Robot Path Control Strategies

After the camera system is implemented, in this section the operational procedure of the tracking system is discussed as shown in **Fig. 9**. The small robot is placed inside a parking area, and the position of the robot is tracked and controlled by C_2 camera. On another side, the sample is observed by a C_1 camera for designing the measurement point. The path that is designed can be obtained

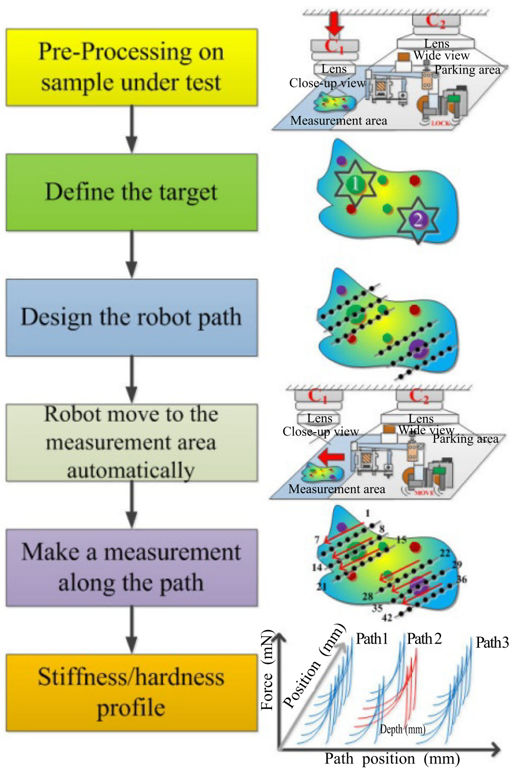

Fig. 9. Measurement process algorithm.

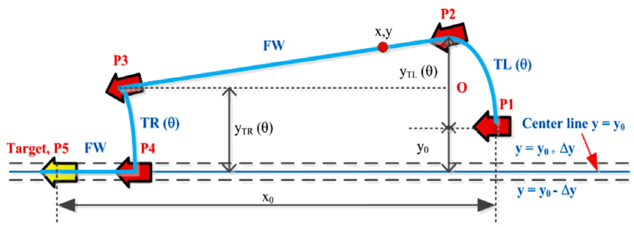

Fig. 10. Robot path design algorithm for wide working range (C_2 camera).

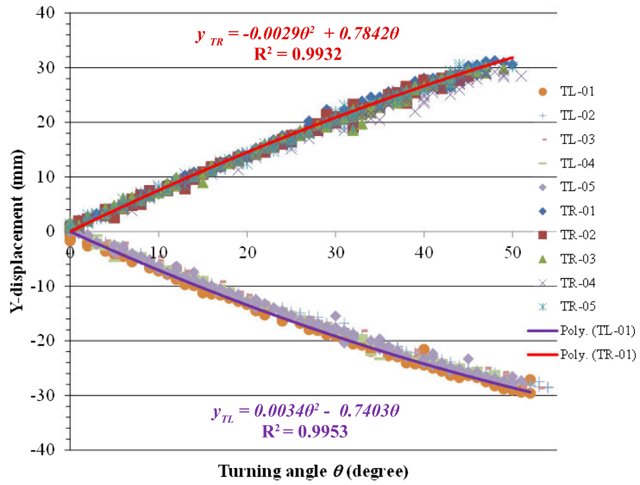

Fig. 11. Turning angle and Y-displacement ability of the robot which is monitored by C_2 camera.

by user or automatically designed by computer. For automatic measurement point part designs, assume that the surface of a sample under test is clean and homogeneous so that the interesting points to make a stiffness measurement are the different texture areas. Computer assigns the most three biggest vivid color pattern on the sample as the measurement points. Then the robot paths are designed to pass through the measurement point one line and outside each top and bottom another line as shown in **Fig. 9**. After a designing of a measurement path point, a C_2 camera provides the coordinate of a robot then computer designs the geometric trajectory path. A robot maneuvered along the designed trajectory path from a parking area to the measurement area automatically, which is controlled by C_2 camera. After a robot would reach the measurement area, a robot makes an indentation along the designed measurement point path, which is controlled by C_1 camera. Finally, the surface stiffness/hardness profile of the measurement areas can be identified.

The robot path control strategies in this research are separated by a camera view and its function, i.e., the wide-range view C_2 camera and the microscopic view C_1 camera. The robot position control procedures on such cameras are different as described in next two sections.

3.1. Path Control for Wide Working Range

The wide-range view C_2 camera as shown in **Fig. 8**, is focused on the left arrow marker placed on the robot. This marker is a representation of the robot position and orientation angle. A robot path control under wide-range view is depicted in **Fig. 10**. The path is produced by a combination of four movement actions, i.e., forward (FW), backward (BW), turn right (TR) and turn left (TL). As discussed in previous paper [9], this small robot is driven by piezo-actuators and electromagnetic legs in a manner of an inchworm. A robot can be turned left or right by supplied a different phase signal to piezo-actuators and the electromagnetic legs simultaneously. Because the joint connected to a front and rear leg together, is not placed at the center of a robot. During a robot is turning, not only its angle is changed but the turning movement also generates a displacement change. Furthermore, a marker cannot place at the position of a pivot point because such point is covered by a robot body. Thus, the relation between turning angle θ and y-displacement change is required in TL and TR directions. Such relation can be determined by a series of turning actions, i.e., each TL or TR will start from $\theta = 0°$ up to $\theta = 50°$ as shown in **Fig. 11**. The standard curve fitting of the relation is shown in Eqs. (1) and (2). These equations are used for calculating the deviation of y-coordinate, which relates to the robot when it turns from 0 to θ [degrees] and vice versa.

$$y_{TL} = 0.0034\theta^2 - 0.7403\theta \quad \quad (1)$$

$$y_{TR} = -0.0029\theta^2 + 0.7842\theta \quad \quad (2)$$

where y_{TL} and y_{TR} are y-displacement corresponding to the orientation of the robot in case of robot turn left and turn right, respectively.

The center line ($y = y_0$) in **Fig. 10**, is the straight line that a robot can reach the target by only moving forward without changing the turning angle θ. To prevent a problem due to slipping movement, the center line requires an upper and lower limit ($\pm\Delta y$) which is specified by the user. Assume that the robot is placed at P1 and its orientation θ should be $\theta = 0°$ (if $\theta \neq 0°$ the robot must turns until $\theta = 0°$), the distance to the target is x_0. A relation of turning angle, shown in **Fig. 11**, indicates that a robot needs at least 30 mm space for turn θ into 50° on both TL and TR movement. For this reason, a distance x_0 (**Fig. 10**) must be larger than 30 mm in case a robot stays out of a center line ($y = y_0$). For example, if the starting position of a robot (P1) is placed near the target (P5), a robot has to move back more than 30 mm. As continued from **Fig. 10**, a robot turns left θ [degrees] from P1 to P2 with distance y-displacement ($y_{TL}(\theta)$) and the smallest turning angle θ calculated by Eq. (1) under the condition that OP3 must be smaller than x_0 in the following equation.

$$\mathrm{OP3} = \frac{\mathrm{OP2}}{\tan\theta} = \frac{y_0 + y_{TL}(\theta) - y_{TR}(\theta)}{\tan\theta} \quad . \;.\; . \quad (3)$$

where θ is the turning angle. OP3 is the displacement from O to P3. OP2 is the displacement from O to P2. y_0 is the displacement from P1 to center line. y_{TL} and y_{TR} are y-displacement corresponding to θ when a of robot turns left and turns right, respectively.

The smallest θ in Eq. (3), is established by increasing θ from 0° until the condition OP3 $< x_0$ is satisfied. Then a robot turns to P2 with such a θ [degree] and moves forward to P3. Assume that the angle of θ is not changed during movement, and the coordinate of a robot is x, y point. The coordinate y of P3 can be determined by the following condition.

$$y_0 - \Delta y < y + y_{TR}(\theta) < y_0 + \Delta y \quad . \;.\; .\; .\; .\; . \quad (4)$$

where Δy is the tolerance limit specified by the user.

The condition in Eq. (4) is checked simultaneously while a robot is moving to P3. When the condition is satisfied, a robot turns right to P4, i.e., a θ [degree] turns to be 0°. With y-displacement $y_{TR}(\theta)$ calculated from Eq. (2), then a robot moves forward from P4 to the target P5 with the x-coordinate defined by

$$x_0 - \Delta x < x < x_0 + \Delta x \quad . \;.\; .\; .\; .\; .\; .\; .\; .\; . \quad (5)$$

where Δx is the tolerance limit specified by the user.

The condition in Eq. (5) is checked simultaneously while a robot is moving to P0. Finally, the condition established by Eq. (5) is a target position. This control algorithm is similar wherever a robot (left arrow) stays below or above the center line.

3.2. Path Control for Microscopic Working Range

A microscopic view C_1 camera has an image with working range 1.8×2.25 mm, as shown in **Fig. 8** which operates on a very small marker size about $100 \times 200\ \mu$m. A main function of C_1 is to track the position of a marker which is running around inside the 1.8×2.25 mm working area. A basic odometry reduction error method is utilized to decrease the deviation between an actual position of the marker and the target position. To reach the target,

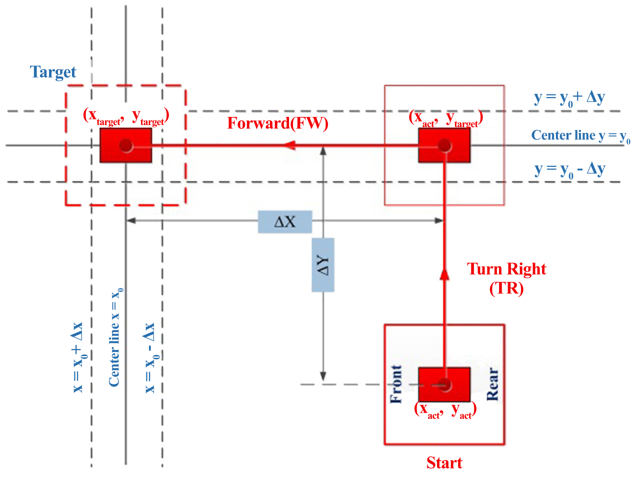

Fig. 12. Robot path design algorithm for microscopic working range (C_1 camera).

the deviation of an actual position and a target must be reduced to zero as shown in Eq. (6). On the way to reach the target, the following Eqs. (7) and (8) are checked simultaneously.

$$\begin{aligned} \Delta X &= x_{act} - x_{target} \\ \Delta Y &= y_{act} - y_{target} \\ 0 &= \Delta X = \Delta Y \end{aligned} \quad . \;.\; .\; .\; .\; .\; .\; .\; .\; .\; .\; . \quad (6)$$

$$y_0 - \Delta y < y_{act} < y_0 + \Delta y \quad . \;.\; .\; .\; .\; .\; .\; .\; . \quad (7)$$

$$x_0 - \Delta x < x_{act} < x_0 + \Delta x \quad . \;.\; .\; .\; .\; .\; .\; .\; . \quad (8)$$

where ΔX and ΔY are the deviation between actual and target position of the marker. (x_{act}, y_{act}) and (x_{target}, y_{target}) are the position of the marker at the actual position and target position, respectively. (x_0, y_0) is the position of the center line of the target position and $\Delta x, \Delta y$ are the upper and lower limit specified by the user.

An example of operation is shown in **Fig. 12**, a robot initially stays at the starting point inside a solid line square (x_{act}, y_{act}), the best way to attain a target inside a dash line square (x_{target}, y_{target}) is to move in forward slanting right direction. However, a mobility of a robot is not precise in such direction, i.e., the movement leads to slip. Therefore, a robot has to move right side to the position (x_{act}, y_{target}) by turning right (TR) within distance ΔY. During left or right movement, Eq. (7) must be satisfied.

Finally, the robot moves forward (FW) within distance ΔX to the target position (x_{target}, y_{target}), during forward (FW) or backward (BW) movement, Eq. (8) must be satisfied.

Here, a robot path control strategies under C_1 microscopic view and C_2 wide range view are described. Then the repeatability of the tracking system by such cameras are determined on the next section.

4. Experiments

To demonstrate the performance of the tracking system, several experiments are presented in this section. The ex-

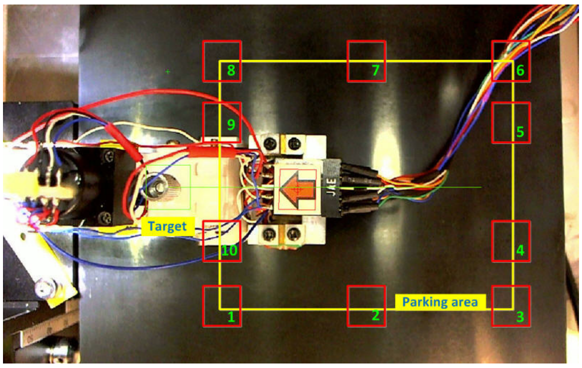

Fig. 13. Experiment setup for wide-range path control.

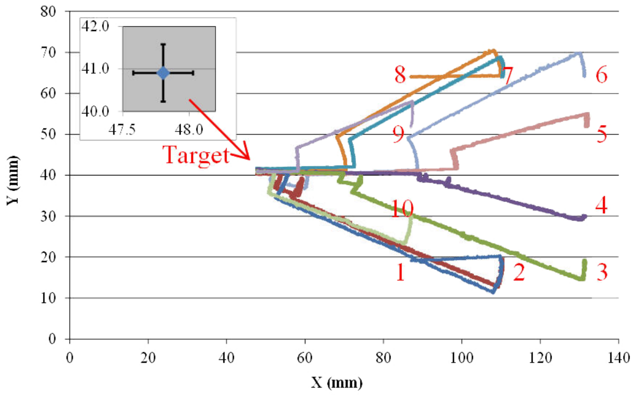

Fig. 14. Repeatability experiment results of wide-range path control.

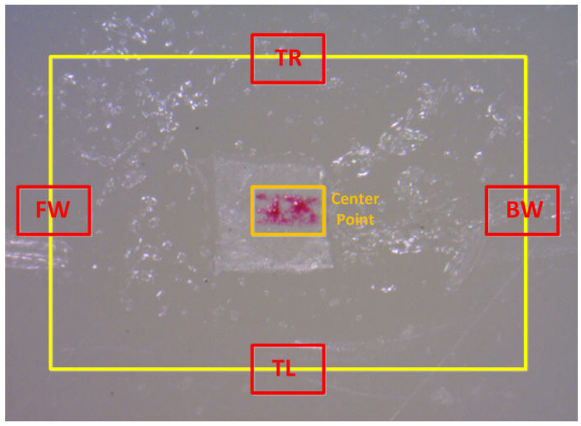

Fig. 15. Experiment setup for microscopic range path control. (In this picture is shows the marker that placed on the top of LVDT case.)

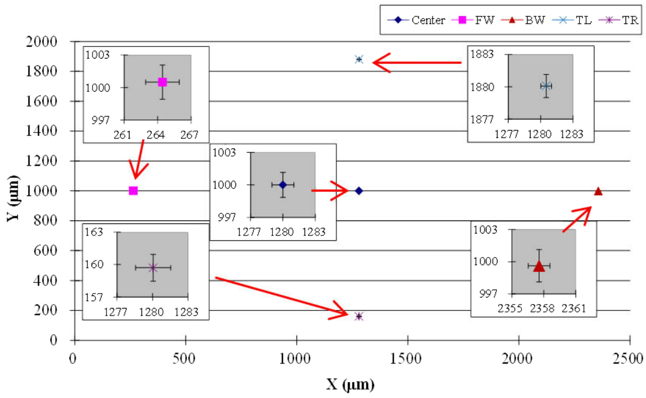

Fig. 16. Repeatability experiment results of microscopic range path control.

periment on a repeatability of a camera system will be described at first. And then the hardness/stiffness measurement performance test will be described at the end of this section.

4.1. Wide-Range Path Control

The reproducibility of the wide-range tracking software can be determined by an experiment setup shown in **Fig. 13**. The testing procedure is carried out by placing a robot at ten specific positions inside a parking area. Then a robot navigates to the target following the robot path and the last position of the robot at the target is recorded. The last position of a robot is a representation of the reproducibility of the tracking system of C_2 camera as shown in **Fig. 14**. The experiment results have shown that, this tracking system achieved ± 1 mm within 150×100 mm working range.

4.2. Microscopic Range Path Control

To carry out the repeatability test of the microscopic view tracking software, a center of a working range is set as a center point. Because a pattern-matching technique can recognize a marker only when its shape is similar to the template. In case of C_1 camera view, when a marker is close to an image border, the shape of which is chanced. Thus, a gap between marker and image border is required to be 100 μm because a marker size is about 200×100 μm. In the experiment, the target is assigned with four positions, FW, BW, TL and TR at the edge of an image with another 100 μm free space as shown in **Fig. 15**. Then a robot navigates into fourth position in ten rounds (go and back) for each position (start from the center point), and the last position of a robot is recorded. The last position of a robot is a representation of the repeatability of the tracking system of C_1 camera as shown in **Fig. 16**. The experiment results have shown that this tracking system achieved ± 3 μm within 2.5×2 mm working range

4.3. Sample Measurement Test

To investigate the performance of the tracking system, we propose one of the most difficult surface hardness investigations on a human tooth sample in this experiment.

Regarding the tooth structure, it is composed of four important layers, i.e., enamel, dentine, cementum and pulp. The enamel is the hardest tissue in the human body and even stronger than bone. Next is the dentine, its layer is similar to the bone. Inside the dentine the pulp occupies at a center, it consists of soft connective tissue and blood vessels. Finally, the cementum that is a mineralized dental tissue covers the roots of the tooth [12].

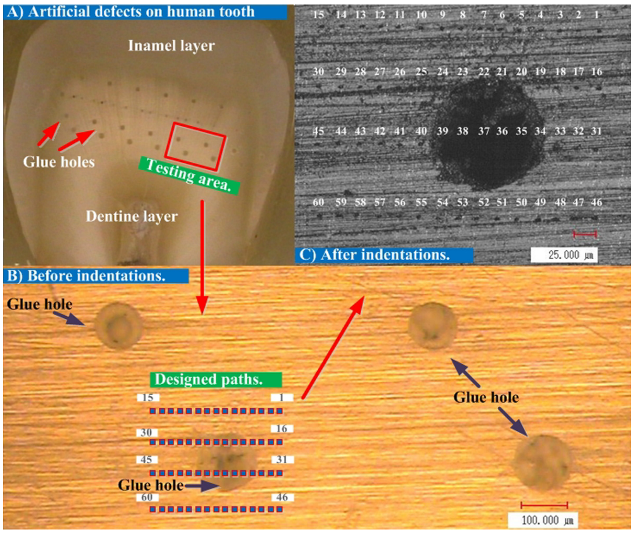

Fig. 17. A) Artificial defects on a human tooth. B) The designed paths on a glue hole of a human tooth. C) The series of indentations scan pass through the glue hole on dentin surface of a human tooth.

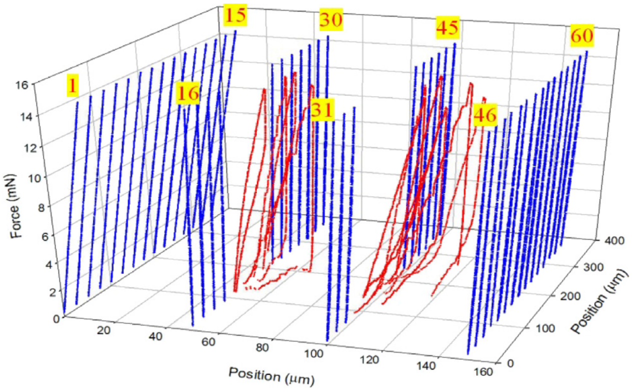

Fig. 18. 3D indentation load-depth curves present the problem area on a human tooth with very deep indentation depth compare with normal tooth surface.

In the experiment, an artificial unhealthy tooth is used to investigate a performance of the tracking system. Such tooth is made from a human tooth 60 years old age source. The series of holes on both enamel and dentine regions of a permanent tooth have been made with 200 μm deep with the 50 μm and 100 μm drill bits shown **Fig. 17A)**. Then the elastomer glue is inserted into all the holes. The glue surface is very soft and high elastic. Therefore, an indentation load-depth characteristic of a glue surface must be different from a normal tooth surface. With the help of an image processing, the measurement path can automatically be designed to pass through a small glue hole on the dentine surface. There are four paths designed, two of which are passed through the glue hole and others of which are placed on the dentine surface. The designed path points with 25 μm separation have been positioned as shown in **Fig. 17B)**. The indentation testing force is fixed at 15 mN and the total dwell time at a maximum force applied is 30 seconds. The close-up picture around an experiment area is shown in **Fig. 17C)**. As experimental results show, load-depth characteristics of the artificial unhealthy tooth surface are summarized in **Fig. 18**, where the different degree of hardness on the different surface characteristic can be checked in this experiment, and several load-depth curves can be identified. The 2nd and 3rd indentation paths which show strange behaviour of the load-depth curves, evidently comes from the effect of a glue hole.

5. Conclusion

The first prototype of a microindentation robot combined with a vision based navigation system has been constructed and described. The simple image processing technique can provide the benefit of a micropositioning surface scan tasks. The repeatability experiment results of a camera system achieved ±1 pixel for both cameras, i.e., ±2.5 μm and ±150 μm for microscopic C_1 camera and wide-range view C_2 camera, respectively. After the camera tracking system is implemented to control a robot position, the accuracy experiment results of a tracking system are achieved ±3 μm and ±1 mm, for C_1 and C_2, respectively. The tracking accuracy with ±1 mm on C_2 camera is good enough to maneuver a robot to a target size 2.5×2 mm. Additionally, the accuracy ±3 μm of C_1 camera is excellent for a measurement part point that is designed within a hundred micrometers separation.

Finally, the performance of a microindentation robot is presented on the results of an unhealthy tooth surface investigation. It is depicted that simple vision based navigation can control the position of a small robot precisely. The robot can get all the measurement points that are designed inside an enclosure chamber. The experimental results indicate that this measurement system can identify a microsurface stiffness on such bio samples, including the inside defect identification. Thus, this machine is considered as the smallest microhardness testing robot in the world.

In the future, the improvement with the hardness measurement performance will be conducted to verify with standard hardness testing machine.

References:

[1] M. Gasko and G. Rosenberg, "Correlation between hardness and tensile properties in ultra-high strength dual phase steels-short communication," Materials Engineering, Vol.18., pp. 155-159, 2011.

[2] Y.-L. Shen and N. Chawla, "On the correlation between hardness and tensile strength in particle reinforced metal matrix composites," Materials science and engineering, A297, pp. 44-47, 2001.

[3] M. A. Salazar-Guapuriche, Y. Y. Zhao, A. Pitman, and A. Greene, "Correlation of strength with hardness and electrical conductivity for aluminum alloy 7010," Materials science forum., Vol.519-521, pp. 853-858, 2006.

[4] J. B. Pethica, "Ion implantation into metals," Proc. of the 3rd Int. Conf. on Modification of Surface Properties of Metals by Ion Implantation, held at UMIST, Manchester, p. 147, 1981.

[5] E. T. Lilleodden, W. Bonin, J. Nelson, J. T. Wyrobek, and W. W. Gerberich, "In situ imaging of μN load indents into GaAs," J. of Materials Research, Vol.10, Issue 09, pp. 2162-2165, 1995.

[6] N. A. Burnham and R. J. Colton, "Measuring the Nanomechanical Properties and Surface Forces of Materials Using an Atomic Force

Microscope," J. of Vacuum Science and Technology A, Vol.7, No.4, p. 2906, 1989.

[7] T. J. Bell, A. Bendeli, J. S. Field, M. V. Swain, and E. G. Thwaite, "The determination of surface plastic and elastic properties by ultra-micro-indentation," Metrologia, Vol.28, No.6, pp. 463-469 1992.

[8] CSIRO Telecommunication & Industrial Physics, Lindfield NSW 2070 Australia, "Ultra-micro indentation system (UMIS)," unpublished.

[9] P. Montree, S. Hirata, C. Kanamori, and H. Aoyama, "Development of microscopic hardness and stiffness investigation system with microrobot," J. of Robotics and Mechatronics, Vol.24, No.1, pp. 123-132, 2012.

[10] S. Fatikow, J. Seyfriend, St. Fahlbusch, A. Buerkle, and F. Schmoeckel, "A Flexible Microrobot-Base Microassembly Station," J. of Intelligent and Robotic Systems, Vol.27, pp. 135-169, 2000.

[11] "IMAQ Vision concept manual," National Instruments, June 2003.

[12] J. K. Avery, "Oral development and history 3rd ed.," Thieme medical publishers Inc., pp. 72-73, 2002.

Name:
Montree Pakkratoke

Affiliation:
Ph.D. Student, Aoyama's Laboratory, Department of Mechanical Engineering and Intelligent Systems, University of Electro-Communications

Address:
1-5-1 Chofugaoka, Chofu, Tokyo 182-8585, Japan

Brief Biographical History:
2003 Received M. Eng. degree from King Mongkut's University of Technology Thonburi, Thailand
2004- Joined the National Institute of Metrology, Thailand
2008- Ph.D. Student, The University of Electro-Communications

Main Works:
• "Development of microscopic hardness and stiffness investigation system with microrobot," J. of Robotics and Mechatronics, Vol.24, No.1, pp. 123-132, 2012.

Name:
Shinnosuke Hirata

Affiliation:
Assistant Professor, Department of Mechanical and Control Engineering, Graduate School of Engineering, Tokyo Institute of Technology

Address:
S5-17, 2-12-1 Ookayama, Meguro-ku, Tokyo 152-8552, Japan

Brief Biographical History:
2009 Received Ph.D. in Eng. degree from Tokyo Institute of Technology
2009- Joined The University of Electro-Communications
2012- Joined Tokyo Institute of technology

Main Works:
• "Improvement of the needle-type dispenser for precise micro-droplet dispensation gap measurement between the needle tip and the target surface based on needle vibration," J. of Robotics and Mechatronics, Vol.24, No.2, pp. 284-290, Apr. 2012.

Membership in Academic Societies:
• The Institute of Electronics Information and Communication Engineers (IEICE)
• The Acoustical Society of Japan (ASJ)
• The Japan Society for Precision Engineering (JSPE)
• The Institute of Electrical and Electronics Engineers (IEEE)

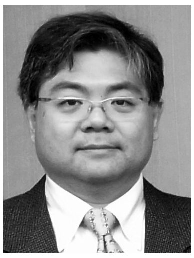

Name:
Chisato Kanamori

Affiliation:
Associate Professor, Department of Mechanical Engineering and Intelligent Systems, Graduate School of Informatics and Engineering, The University of Electro-Communications

Address:
E4-303, 1-5-1 Chofugaoka, Chofu-shi, Tokyo 182-8585, Japan

Brief Biographical History:
1987 Received B.E from The University of Electro-Communications (UEC)
1989 Received M.E from UEC
1991- Research Associate, UEC
2004 Received D.E from UEC
2005- Associate Professor, UEC

Main Works:
• "Development of Intelligent Encoder," Proc. of The Twenty-third Annual Meeting of The American Society for Precision Engineering and the Twelfth ICPE (CD-ROM), No.2639, p. 4, Portland, USA, Oct. 21, 2008.

Membership in Academic Societies:
• The Japan Society of Mechanical Engineers (JSME)
• The Japan Society of Precision Engineering (JSPE)
• The Robotics Society of Japan (RSJ)

Name:
Hisayuki Aoyama

Affiliation:
Professor, Department of Mechanical Engineering and Intelligent Systems,The University of Electro-Communications

Address:
E4-304, 1-5-1 Chofugaoka, Chofu, Tokyo 182-8585, Japan

Brief Biographical History:
1983- Research Laboratory of Precision Machinery and Electronics, Tokyo Institute of Technology
1988- Department of Precision Engineering, Shizuoka University
1997- Department of Mechanical Engineering and Intelligent Systems, The University of Electro-Communications

Main Works:
• "Precise miniature robots and desktop flexible production," Proc. of Int. Workshop on Micro Factory, pp. 149-156, 1998.

Membership in Academic Societies:
• The Japan Society of Precision Engineering (JSPE)
• The Japan Society of Mechanical Engineering (JSME)
• American Society for Precision Engineering (ASPE)
• The Robotics Society of Japan (RSJ)